Colloid Polym Sci (2005) 283: 1267–1277
DOI 10.1007/s00396-005-1334-1

ORIGINAL CONTRIBUTION

M. Lansalot
M. Sabor
A. Elaissari
C. Pichot

Elaboration of fluorescent and highly magnetic submicronic polymer particles via a stepwise heterocoagulation process

Received: 28 September 2004
Accepted: 31 March 2005
Published online: 10 August 2005

M. Lansalot · M. Sabor · A. Elaissari
C. Pichot (✉)
Systémes Macromoléculaires
et Physiopathologie Humaine,
UMR 2714 - 46, allée d'Italie,
69364 Lyon Cedex 07, France
E-mail: christian.pichot@ens-lyon.fr
Tel.: +33-4-72728739

Abstract Using the stepwise heterocoagulation concept, fluorescent and highly magnetic submicronic core-shell polymer particles were prepared. For this purpose a negatively charged oil-in-water magnetic emulsion was first modified by adsorbing the poly(ethyleneimine) (PEI). Secondly, low glass transition temperature ($T_g = 10°C$) anionic film-forming nanoparticles were adsorbed onto the cationic magnetic droplets. Finally the encapsulation was induced by heating the heterocoagulates above the T_g of the film-forming nanoparticles. To produce labeled magnetic particles, fluorescent nanoparticles and film-forming nanoparticles were simultaneously adsorbed. PEI adsorption was investigated. Also investigated was the influence of the amount of film-forming nanoparticles and fluorescent nanoparticles on the encapsulation efficiency.

Keywords Heterocoagulation · Submicronic particles · Magnetic emulsion · Fluorescent

Introduction

In the last decade, magnetic particles have evoked increasing interest in various applications, especially in the diagnostic field [1]. The most attractive feature of these particles is their rapid extract ability by magnetic separation. For biomedical applications, magnetic particles should fulfill various criteria. Particle size, particle size distribution and appropriate surface functionalities for further selective binding need to be finely controlled. Moreover, the magnetic material has to be properly encapsulated in order to avoid any leakage of iron oxide. To meet these requirements, many routes have been designed [2]. Some of them involve polymerization techniques [3–6] others more physicochemical methods such as the layer-by-layer deposition technique [7, 8] or the stepwise heterocoagulation [9, 10]. This last process, which more often relies on electrostatic interactions to induce the coating of small particles onto large ones, was pioneered by Vincent et al. [11] and Ottewill et al. [12, 13] for the adsorption of small cationic PS particles onto large anionic PS ones. Later, Furusawa et al. [14] applied this concept to the elaboration of silica-latex composite particles. It was further developed by Okubo et al. [15] and Ottewill et al. [16] to prepare particles with controlled morphologies. The first report on the preparation of magnetic particles via heterocoagulation process came from Furusawa et al. [9]. This process consisted in: (1) the adsorption of magnetic nanoparticles ($NiO.ZnO.Fe_2O_3$, 20 nm diameter) onto oppositely charged polystyrene submicronic particles and (2) the encapsulation (via radical polymerization of styrene in the presence of a charged surfactant) of the magnetic layer in order to avoid the release of the adsorbed magnetic material. Such a process was later used by Sauzedde et al. [10] who carried out the adsorption of iron oxide nanoparticles onto oppositely charged core-shell particles (polystyrene core and slightly crosslinked poly(*N*-isopropylacrylamide) shell). The adsorption step was performed as reported by Furusawa [9], whereas the encapsulation step was investigated via surfactant-free radical polymerization using *N*-isopropylacrylamide as

the main monomer, methylene bisacrylamide as a crosslinker and potassium persulfate as the initiator. Compared to Furusawa's process, the amount of iron oxide incorporated into the corona of the core-shell latexes was found to be higher due to the adsorption within the hairy layer of the particles rather than onto smooth polymer surfaces. It is worth noting that the methods reported so far in the literature are mainly devoted to the synthesis of large magnetic particles (i.e. diameter larger than 500 nm). Only a few works have dealt with the preparation of smaller particles highly loaded with iron oxide although the corresponding colloids are of particular interest. Indeed, they would offer low sedimentation rate and a large specific surface area for non-specific or specific binding of biomolecules.

In order to prepare submicronic highly magnetic (and fluorescent) polymer particles, we designed and implemented a new strategy based on a stepwise heterocoagulation process (see Scheme 1). Two previous papers [17, 18] reporting on the synthesis of polymer core-shell particles by stepwise heterocoagulation using small coating particles with low glass transition temperature T_g were advantageously used as models for our purpose. In the context of our study, the first colloid is a relatively monodisperse oil-in-water magnetic emulsion, and the second one is a negatively charged film-forming nanolatex. In some cases, this nanolatex is used together with fluorescent carboxylic polymer nanoparticles since fluorescent magnetic particles may be very attractive for some specific biomedical applications. After the adsorption of the small nanoparticles onto the modified magnetic droplets, the heterocoagulates obtained are heated above the T_g of the film-forming nanolatex to form a homogeneous polymer shell. Such a process does not require any additional (or final) polymerization step compared to the above reported approaches [9, 10]. The final magnetic particles may be used as a solid support for further immobilization of biomolecules such as nucleic acids or antibodies.

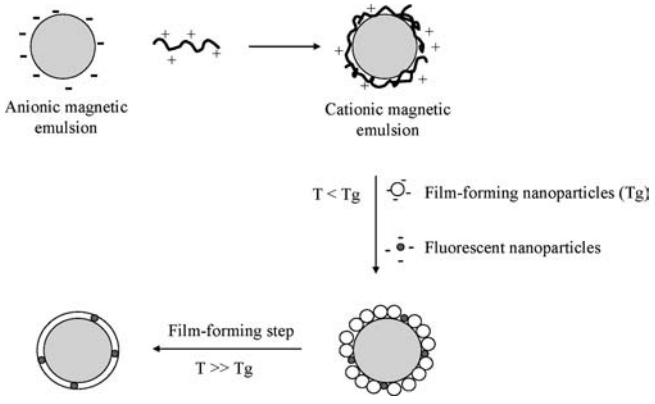

Scheme 1 Stepwise heterocoagulation process used to form magnetic particles

Experimental

Materials

Deionized water (Millipore Milli-Q purification system) was used in the entire study. Magnetic emulsions and film-forming nanoparticles (Rhodopas Ultrafine PR 3500) were kindly provided by Ademtech SA (Pessac, France) and Rhodia (Aubervilliers, France), respectively. The fluorescent nanoparticles (FluoSpheres F-8787, from Molecular Probes), polyethyleneimine (PEI, $M_w = 25{,}000$ g/mole, branched, from Aldrich) and a modified polyacrylic acid-based amphiphilic graft copolymer (Coatex M883, $M_w = 50{,}000$ g/mol, 21 wt%; critical aggregation concentration = 1.4 g/L at pH9), kindly provided by Coatex (Lyon, France), Scheme 2) were used as received. The main features of the oil-in-water magnetic emulsions are listed in Table 1. Chemical composition and colloidal characterization were recently reported by Montagne et al. [6, 19]. The synthesis can be briefly described as follows: an organic ferrofluid composed of iron oxide nanoparticles stabilized in octane by a surrounding oleic acid layer, was emulsified in water with nonionic surfactants (nonylphenol ether (NP10) and *t*-octylphenoxypolyethoxyethanol (Triton X-405)). Table 2 displays the characteristics of the film-forming and fluorescent nanoparticles.

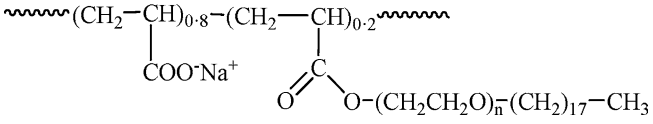

Scheme 2 Modified polyacrylic acid-based amphiphilic graft copolymer (Coatex M883)

Table 1 Features of the magnetic emulsions used in this study

Reference	ME1	ME2
D_h (nm)[a]	246	249
D_n (nm)[b]	219	221
D_w (nm)[b]	233	232
Polydispersity index[b]	1.066	1.050
Solid content (%)	6.1	9.7
Density (g cm^{-3})[c]	2.66	2.42
Magnetite content (wt%)[c]	70	70

[a]From dynamic light scattering
[b]From TEM photos

Table 2 Features of film-forming and fluorescent nanoparticles used in this study

Reference	Rhodopas PR 3500	Yellow-green fluospheres
D_h (nm)[a]	47	24
Polymer nature	Acrylic copolymer ($T_g \sim 10°C$)[b]	Polystyrene ($T_g \sim 100°C$)[c]
Density (g cm^{-3})	1.03[d]	1.04[c]
Fluorescence	/	$\lambda_{exc} = 505$ nm[e] $\lambda_{em} = 515$ nm[e]

[a]From dynamic light scattering
[b]Measured by differential scanning calorimetry
[c]According to reference 31
[d]Provided by Rhodia

Preparation of the cationic magnetic emulsion

Two milliliter of deionized water were added to either 2 mL (ME1) or 1.2 mL (ME2) of anionic magnetic emulsion and the mixture was homogenized by vortex mixing. After magnetic separation, the supernatant was removed and the magnetic droplets were then dispersed in 4 mL of water. Following a further step of homogenization and magnetic separation, 2 mL of water was added. After redispersion, this 2 mL of washed magnetic emulsion was added to 4 mL of a PEI solution. After 15 min of stirring, the magnetic droplets were washed two times using 4 mL of water, before final redispersion in 2 mL of water.

Polyethyleneimine adsorption study

The amount of PEI adsorbed onto the magnetic droplets was deduced by titrating the free PEI via specific amine titration using fluorescamine [20] (Scheme 3). The fluorescent product obtained was quantified using fluorescence spectrophotometer (LS 50 system, Perkin Elmer).

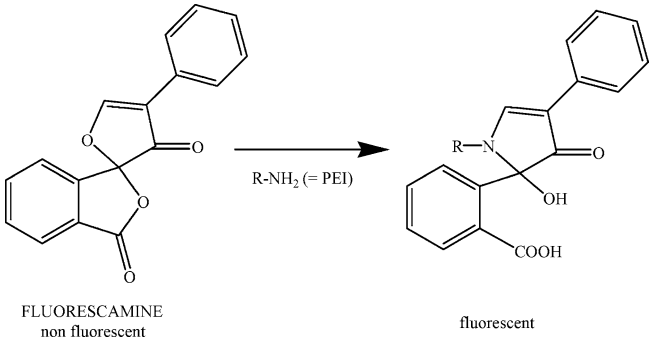

Scheme 3 Specific amine titration using fluorescamine

A calibration curve was first established (emission intensity measured at 472 nm for an excitation wavelength of 388 nm). The procedure was as follows: PEI standard solutions in milli-Q grade water were prepared, ranging from 0.1 mg mL^{-1} to 1 mg mL^{-1}. Standard solution of volume 100 μL was added to 2.9 mL of 0.01 M borate buffer pH 9.1, then 1 mL of 0.3 mg mL^{-1} fluorescamine solution in acetone was also added. The PEI amino groups and fluorescamine were then allowed to react for 24 h in the dark. ME1 was used for this study, with all the quantities adjusted in order to use low volumes (100 μL) rather than 2 mL. The concentration of PEI solutions ranged from $C_0 = 0.1$ to 25 mg mL^{-1} for a pH between 8 and 11 depending on PEI concentration. After the PEI adsorption step, 100 μL of supernatant was withdrawn and allowed to react with fluorescamine following the procedure described above. The adsorbed amount N_{ADS} (mg m^{-2}) was finally calculated from Eq. 1:

$$N_{ADS} = V \times \frac{C_i - C_f}{mA_{SP}}, \quad (1)$$

where V (mL) in the total volume of the adsorption medium, C_i (mg mL^{-1}) and C_f (mg mL^{-1}) the initial and the final concentrations of PEI solution in the reaction medium, respectively, A_{SP} (m^2 g^{-1}) the specific surface area of the magnetic droplets and m (g) the mass of dried magnetic emulsion.

A subsequent series of adsorption experiments was performed with 5 mL samples, i.e. in the same order of magnitude as the one used in the heterocoagulation experiments. The effect of PEI concentration on the preparation of cationic magnetic emulsion was studied using four different PEI concentrations (1, 10, 25 and 50 mg mL^{-1}). The influence of the pH was also investigated by adjusting the pH of the PEI solutions before adsorption using the HCl 1 M.

Heterocoagulation step

The film-forming nanoparticles and 10^{-3} M NaCl (such that the total volume was 20 mL) were placed in a 100 mL thermostatted reactor. The pH was first adjusted to 7 with 1 M HCl. The cationic magnetic emulsion (2 mL) obtained in the former stage was mixed with 12 mL of 10^{-3} M NaCl (pH 7), and continuously added (20 mL h^{-1}) to the reactor content. The temperature was set at 2°C during the heterocoagulation process. In some cases, fluorescent polystyrene-based nanoparticles were added together with the film-forming ones in order to prepare labeled magnetic particles. As a systematic study, different ratios R of small particles number to large particles number were investigated:

$$R = \frac{N_S}{N_L} \quad (2)$$

with N_S and N_L being the number of small particles (i.e. the film-forming ones) and the number of large particles (i.e. the magnetic droplets), respectively. When fluorescent particles were introduced together with the film-forming ones, R was redefined with N_S as the sum of the film-forming and the fluorescent particles. We also used the ratio R_f defined as

$$R_f = \frac{\text{number of fluorescent nanoparticles}}{\text{number of film-forming nanoparticles}} \quad (3)$$

Film-formation step

Magnetic heterocoagulates (magnetic emulsion droplets surrounded by polymer nanoparticles) were separated from the supernatant via magnetic separation and then dispersed in a solution of the amphiphilic copolymer Coatex M883 (0.8 g L^{-1} of 0.01 M borate buffer solution). After a second magnetic separation, the heterocoagulates were redispersed in Coatex M883 solution, then placed in the reactor heated at 50°C (temperature above the T_g of the film-forming nanoparticles), and stirred for 20 h.

Characterization

Particle size analysis

The hydrodynamic diameter was obtained by dynamic light scattering (DLS) (Zetasizer 3000HS, from Malvern Instruments). The particle size distribution and the particle morphology were examined by scanning electron microscopy (Hitachi S800) and transmission electron microscopy (Philips CM 120).

Electrophoretic mobility

The electrophoretic mobilities at different stages of the heterocoagulation process were measured as a function of the pH (10^{-3} M phosphate buffer) using a Zetasizer 3000HS (Malvern Instruments). Each value was the average of five measurements. The measured electrophoretic mobilities were then converted into zeta potentials (ζ) using Smoluchowski's [21] equation.

Fluorescence analysis

Imaging was performed with a Zeiss Axioplan 2 Imaging microscope, equipped with a camera and a 100X infinity-corrected 1.3 numerical aperture oil objective. For fluorescence observations, an Hg lamp was used in combination with a filter set for fluorescein.

The fluorescence emitted by the final magnetic particles was quantified by flow cytometry using a FACScalibur (BD Bioscience, Becton Dickinson).

Thermogravimetric analysis

The amount of magnetic material in the final dispersion was determined by thermogravimetric analysis (TGA). Measurements were performed under a nitrogen atmosphere at a heating rate of 10°C min^{-1} from 20°C to 550°C (DuPont Instruments TGA 2950 Thermogravimetric Analyzer).

Results and discussion

Preparation of the cationic magnetic emulsion

To induce the adsorption of the small anionic nanoparticles onto the anionic magnetic droplets, the charge of the magnetic emulsion had first to be reversed by the adsorption of a polycation (PEI). Thus, the first step of this work was a preliminary study on PEI adsorption onto the anionic droplets of the magnetic emulsion ME1. The adsorption isotherm obtained is displayed in Fig. 1. Values presented in this plot correspond to initial concentrations of PEI, C_0 ranging from 0.1 mg mL^{-1} to 10 mg mL^{-1}. A plateau was reached for an adsorbed amount of PEI (N_{ADS}) at around 6 mg m^{-2} . However, only concentrated PEI solutions (above 25 mg mL^{-1}) led to stable magnetic emulsion. In order to elucidate this behavior, further adsorption experiments were carried out, working with 5 mL samples (which was of the same order of magnitude as in the proper stepwise heterocoagulation experiments). Four different PEI concentrations (1, 10, 25 and 50 mg mL^{-1}) and the influence of the pH were investigated (Table 3). For PEI concentration of 1 mg mL^{-1}, irreversible aggregation was observed, whatever the pH. When the concentration was raised to 10 mg mL^{-1}, partial aggregation was observed. For higher PEI concentrations (≥ 25 mg mL^{-1}), stable magnetic droplets were obtained only at alkaline pH.

Poly(ethyleneimine) protonation and thus its adsorption are complex phenomena as this molecule displays branched structure and multiple pKa [22, 23] with a pH dependent degree of protonation. The percentage of amino groups protonated as a function of the pH as measured by Hostetler et al. [24] were considered (see Table 3). At acidic pH, PEI molecules are fully dissociated and likely display a stretched conformation as a consequence of intra-repulsive electrostatic interactions, and they should strongly adsorb onto the magnetic droplets (ζ potential ca. −15 mV). However,

Table 3 Features of PEI adsorption on ME1

[PEI] (mg mL^{-1})	pH = 5 ($\alpha \sim 62$)[a]	pH = 7 ($\alpha \sim 45$)[a]	pH = 9 ($\alpha \sim 18$)[a]	pH = 11 ($\alpha = 0$)[a]
1	Aggregation			
10	Aggregation	Progressive aggregation		
25	Aggregation	A few aggregates	Stable	
50				

[a] α is the % of amino groups protonated according to ref [24] (measured in 0.1 M NaCl solution for $M_w = 18{,}000$ g/mol)

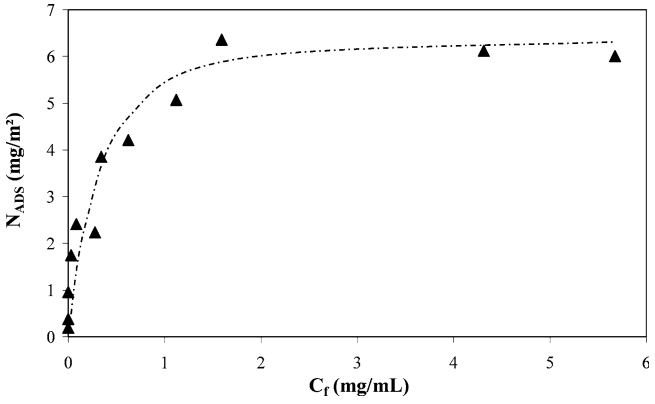

Fig. 1 Adsorption isotherm of PEI onto anionic magnetic droplets ME1

whatever the PEI concentration, systematic aggregation was observed at low pH. This behavior could depend on the PEI concentration. For low PEI concentration, either surface charge neutralization was reached or PEI concentration was too low to avoid bridging flocculation of magnetic droplets. For high PEI concentration, stretched PEI molecules may strongly adsorb onto the droplets by establishing a great number of contacts with the surface, but repulsive electrostatic interactions between adsorbed PEI molecules (lateral interaction) and/or between adsorbed PEI molecules and PEI chains in free solution prevented further adsorption.

In the pH 11 region, the degree of protonation is close to zero thus minimizing repulsive interactions between and within PEI molecules which are believed to exhibit a coil structure with an approximately 10 nm diameter [25]. Due to the absence of charges on PEI molecules, adsorption via hydrogen bonding between PEI amino groups and carboxyl and hydroxyl groups located at the surface of the magnetic droplets may likely be the predominant mechanism. Indeed, the surface of the magnetic droplets is coated with (1) carboxyl groups coming from oleic acid and (2) hydroxyl groups coming either from the surface of iron oxide nanoparticles located close to the interface [6], or from the nonionic surfactants (NP10 and essentially Triton X-405 which displays a high HLB). Hydrogen interactions may induce adsorption of PEI but the adsorbed molecules would not be able to stabilize the magnetic droplets owing to (1) the absence of charge (no electrostatic stabilization) and (2) the adsorption of PEI molecules as compact spheres or as entangled chains providing poor steric stabilization. That would explain why the system was not stable for low PEI concentration. Nevertheless, when increasing this concentration, non adsorbed polymer molecules may arrange themselves between the droplets ensuring stabilization of the suspension by depletion. This excess of PEI chains seems to be necessary to obtain stable magnetic emulsion at pH 11.

pH 7 and pH 9 represented intermediate situations for which the PEI adsorption may be attributed to a combination of both electrostatic interactions and hydrogen bonding. Each of this interaction may be predominant depending on the pH and PEI concentration. However, stabilization was not ensured, except for pH 9 and high PEI concentration.

Although this preliminary study needs further investigation to fully understand the phenomena operating in this system, dispersion exhibiting good colloidal stability was obtained for PEI concentration of 50 mg mL^{-1} and pH 11. Figure 2 displays the ζ potential variation as a function of pH for the magnetic seed and for PEI containing magnetic emulsion. The corresponding droplets size for the cationic droplets is around 315 nm. Based on these results, a PEI concentration of 50 mg mL^{-1} was finally adopted for the rest of the study.

Encapsulation of the magnetic emulsion by film-forming nanoparticles

Once the cationization step optimized, the adsorption of film-forming nanoparticles onto the cationic magnetic droplets was investigated. Since a large difference between the charges of the two colloids should be the driving force for an efficient heterocoagulation, the pH for adsorption was fixed at 7, value for which the zeta potentials of the nanoparticles and the cationic magnetic droplets were -50 and $+25$ mV, respectively (Fig. 2). Furthermore, magnetic particles exhibit the great advantage that all purification and separation steps were facilitated. Hence, the excess of non adsorbed film-forming nanoparticles could easily be removed before the proper encapsulation step. Preliminary studies showed that the heterocoagulates needed to be post-stabilized before inducing this film-formation step. This was achieved by washing the heterocoagulates with an alkaline solution of the amphiphilic surfactant Coatex M883 bearing carboxylic groups (which may also allow further covalent binding of biomolecules). Moreover, taking into account previous works [18, 26] the film-formation step was carried out by incubating the hete-

rocoagulates for 20 h at 50°C (above the T_g of the film-forming nanoparticles). The efficiency of the heterocoagulation and the film-formation processes was assessed by examining the final particle size, the ζ potential and the morphologies of the encapsulated magnetic droplets.

The first series of experiments performed with ME1 aimed at finding the best ratio $R = N_S/N_L$ (See Experimental Part). The cationization step was well controlled since the size of the cationic droplets was reproducible (Table 4). However, a different behavior was observed for the proper heterocoagulation step. A ratio R lower or equal to 330 was not sufficient to produce stable heterocoagulates since systematic aggregation was observed. Dispersion of the elaborated magnetic units after the addition of the amphiphilic copolymer solution was impossible. This phenomenon may be related to the simultaneous adsorption of the same nanoparticle onto more than one magnetic droplet (i.e. bridging flocculation). In contrast to these results, stable systems were obtained for $R = 730$ or higher. The best compromise between particle size, particle size distribution and amount of film-forming nanoparticles was actually achieved for $R = 730$.

The zeta potential variation as a function of the pH (Fig. 3, $R = 730$) indicates that the expected changes in the surface charge of the magnetic units after each significant step of the process had effectively occurred. It is worth noting that the addition of the amphiphilic copolymer induced a lowering of the zeta potential (ca. 25 mV difference, whatever the pH). In addition, no variation of the zeta potential was observed after the spreading of the film-forming nanoparticles. The amphiphilic copolymer still efficiently stabilized the particles after the film-formation, which suggests that even if it could be embodied in the acrylic film, the carboxylic functions were still available to ensure electrostatic stabilization. If the adsorption step of the amphiphilic copolymer was suppressed, the dispersion of the encapsulated magnetic particles after only one magnetic separation was not feasible. The final particle size distribution and the effective encapsulation of the magnetic core were checked by electron microscopy (Fig. 4). The number average diameter $\overline{D_n} = 262$ nm calculated from the TEM photos (not shown; polydispersity index = 1.074) agrees well with $D_h = 270$ nm (Table 4) obtained from DLS measurement. The shell thickness would be around 25 nm according to DLS and around 40 nm according to TEM. This last value is likely to be the most reliable one, since $\overline{D_n}$ values are more accurate than D_h ones.

With a view to improve the particle size distribution, the experiment for which $R = 730$ was repeated using ME2 magnetic emulsion, which exhibits lower polydispersity than ME1 (see Table 1 and Fig. 5). In fact, even if the average final particle size was the same for the two experiments (270 nm), the particle size distribution of the final magnetic particles obtained from ME2 was narrower than the one obtained from ME1 (PDI = 1.047 versus PDI = 1.074). The following experiments were therefore carried out with the ME2 batch. In an attempt to further decrease the number of film-forming nanoparticles, an experiment was performed with ME2 and $R = 500$. The magnetic particles obtained exhibited the same diameter as for $R = 730$. This fact suggests that the

Table 4 Evolution of the hydrodynamic diameter (nm) for the magnetic units after each step of the process for 4 different ratios R

Exp.	Cationic droplets	Het. Units + Amphiphilic Copolymer	Final magnetic particles
$R = 110$	324	Aggregates	Aggregates
$R = 330$	313	Aggregates	Aggregates
$R = 730$	317	281	270
$R = 1{,}500$	316	265	260

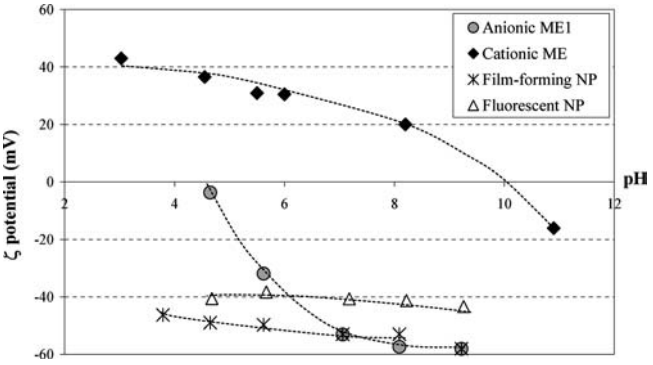

Fig. 2 Evolution of the ζ potential as a function of the pH for the anionic magnetic emulsion ME1 (*filled circle*); the cationic magnetic emulsion obtained with [PEI] = 50 mg mL^{-1} and pH 11 (*filled diamond*); the film-forming nanoparticles (*asterisk*); the fluorescent nanoparticles (*open triangle*). *Dotted lines* are guide for the eyes only. *NP* Nanoparticles

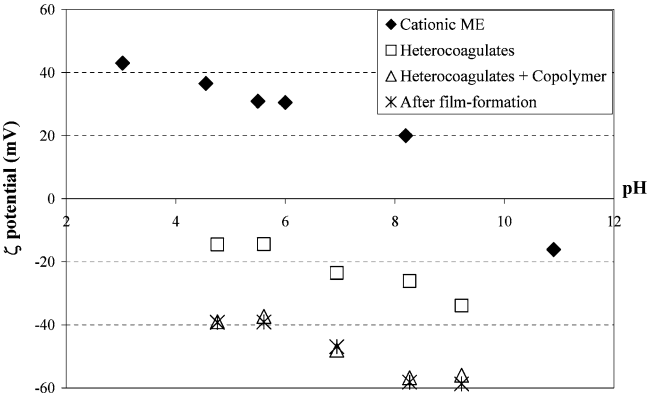

Fig. 3 Evolution of the ζ potential as a function of the pH for $R = 730$ and [PEI] = 50 mg mL^{-1}

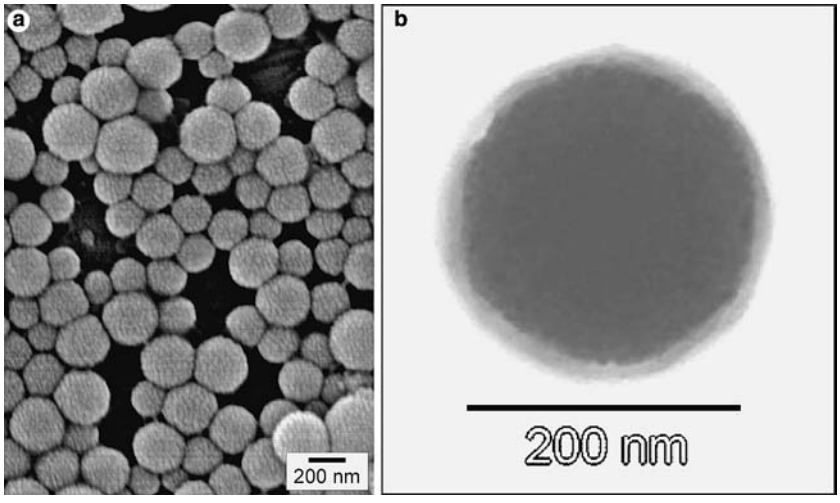

Fig. 4 **a** SEM and **b** TEM photos of the final magnetic particles obtained for $R = 730$

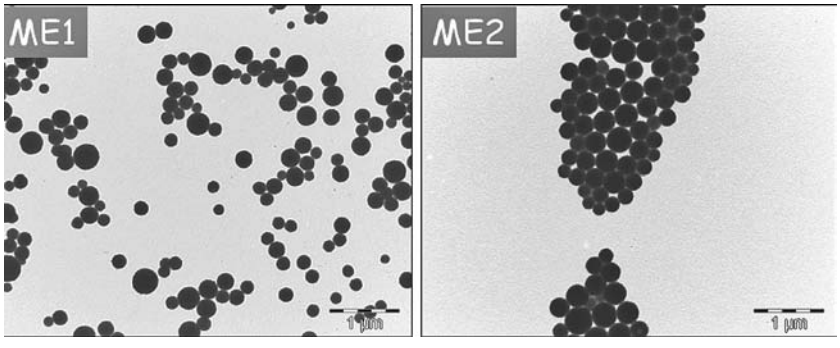

Fig. 5 TEM photos of the magnetic emulsions ME1 and ME2

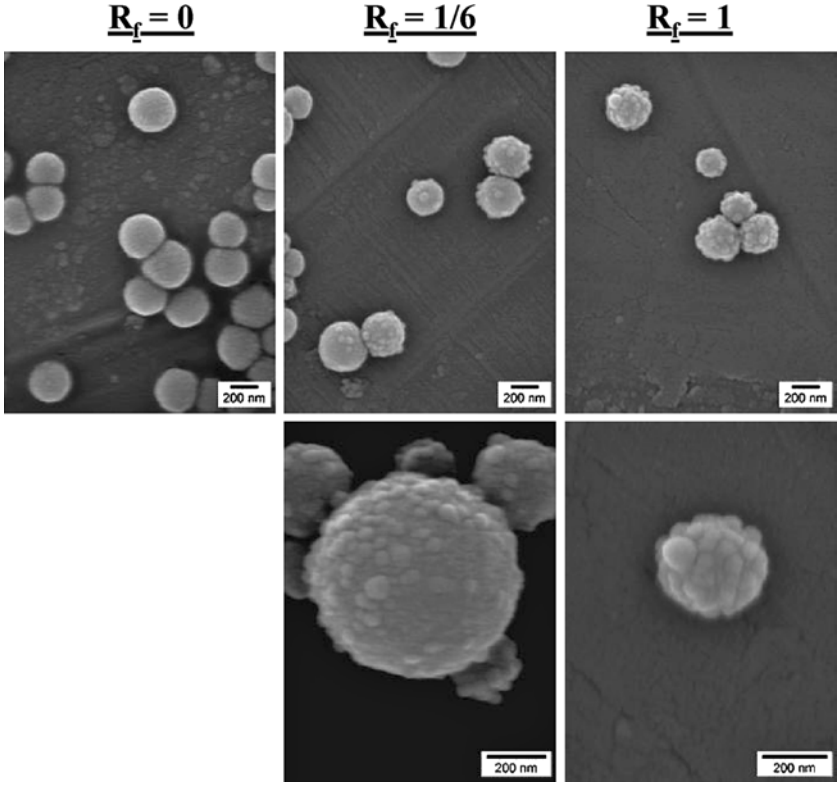

Fig. 6 SEM photos of magnetic particles obtained in the absence ($R_f = 0$) and in the presence ($R_f = 1/6$ and $R_f = 1$) of fluorescent nanoparticles ($R = 500$)

film-forming nanoparticles were in large excess for $R = 730$.

Some of the works reported in the literature have tried to determine the optimum ratio R of the number of small to large particles, or to predict the maximum number of adsorbed small particles per large particle N_{sat} [17, 27]. Different parameters have to be taken into account such as the particle size of the two types of particles or the hydrophilic-hydrophobic character of their surface. The body of the theory was developed on the basis of a hexagonal close-packed monolayer of small particles assuming a sphere-on-plane geometry, and the following equation was found to adequately predict N_{sat} [27]:

$$N_{sat} = \frac{2\pi}{\sqrt{3}}\left(1 + \frac{R_L}{R_S}\right)^2 \quad (4)$$

where R_L and R_S are the radii for large and small particles, respectively.

However, as demonstrated by Li et al. [26], when the size ratio between the radii of large to small particles is not high enough (i.e. $2 \leq R_L/R_S \leq 10$), the curvature of the large particle cannot be neglected and one must assume a sphere-on-sphere geometry. Hence the former expression of N_{sat} could be no longer valid. In our system, assumption of a sphere-on-plane geometry would lead to $N_{sat} = 145$. However, as experimentally observed, efficient heterocoagulation occurred only for higher N_S/N_L ratio ($R > 330$). The system investigated in this work would then more likely follow a sphere-on-sphere geometry, especially as $R_L/R_S \approx 5$. In addition, other features of this system could also explain this discrepancy with the theory usually assumed of the sphere-on-plane geometry. Firstly, the systems described in the literature relied on a "batch" mixing of the two types of particles to heterocoagulate, i.e. the dispersions of each type of particles were mixed together and allowed to coagulate for various periods. The protocol was quite different in our case, as cationic magnetic droplets were continuously added to the nanoparticles dispersion. Secondly, various polymeric stabilizers (such as non ionic polyoxyethylene sorbitan monoleate (Tween 80) [18], polyethyleneglycol derivative [16], poly(vinyl alcohol) [26, 28, 29] hydroxyl propyl cellulose [26], polyethylene oxide [29] or poly(vinyl pyrrolidone) [29]) were used to stabilize the particles (large, small, or both). Even if the heterocoagulation induced partial or complete neutralization of the surface charges thus decreasing the electrostatic stabilization, the colloidal stability of the heterocoagulates could still be sterically ensured by the hydrophilic polymer. This was not the case in our system justifying that magnetic heterocoagulates need to be post-stabilized by the amphiphilic copolymer. Moreover, the size distribution of the initial magnetic emulsion was not as narrow as those of the large particles used in the studies described in the literature. Hence, the specific surface area may be greater than expected especially as small magnetic droplets were clearly visible on the TEM photo (Fig. 5). That would explain why a ratio $R = 330$ was not sufficient to cover the magnetic droplets individually. Finally, another parameter which must be considered is the total weight concentration C_w of the magnetic droplets and film-forming nanoparticles. As discussed by Li et al. [29], it could be difficult to find a good balance between inefficient heterocoagulation and aggregation. The higher the C_w, the higher is the probability of heterocoagulation. However, too high a C_w could lead to the formation of aggregated heterocoagulate units. On the other hand, the range of C_w values for which the expression of N_{sat} is valid was not mentioned [27]. For the system studied here, $C_w = 0.9$, but this value was not optimized.

In order to elucidate these discrepancies with the theory, it will be of interest to observe the heterocoagulates via electron microscopy before the film-formation step. Moreover, the degree of coverage θ defined as $\theta = N_{ads}/N_{sat}$ with N_{ads} the number of small particles effectively deposited onto the large ones, was not evaluated in this first series of experiments. These two studies would help to determine how the nanoparticles adsorb onto the magnetic ones.

Encapsulation of the magnetic emulsion by film-forming nanoparticles and fluorescent nanoparticles

The results obtained in the previous section showed that a ratio $N_S/N_L = 500$ was enough to form magnetic heterocoagulates, which have been subsequently and successfully encapsulated by the spreading of the small film-forming nanoparticles above their T_g. In this section, fluorescent carboxylic polystyrene nanoparticles have been used together with the film-forming ones. Indeed, the aim in the next series of experiments was to prepare fluorescent magnetic particles. The ratio $R = N_S/N_L$ was redefined, with N_S as the sum of the film-forming and the fluorescent nanoparticles. R was kept constant at 500 while varying the respective amounts of film-forming and fluorescent nanoparticles, i.e. R_f.

With regard to the surface charge, the expected charge inversion after each step of the process was observed in all the experiments performed. The values of the ζ potential were independent of R_f. On the contrary, the initial value of R_f had a significant influence on the final particle size of the magnetic particles (Table 5). The higher the proportion of fluorescent nanoparticles, the higher was the final diameter. This increase in the size was directly related to the nature of the fluospheres. Indeed, these polystyrene nanoparticles displayed a T_g [30] higher than the temperature applied to induce the

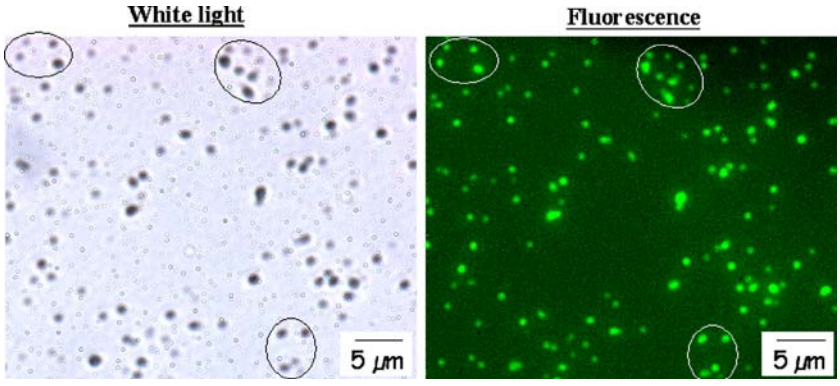

Fig. 7 Fluorescence imaging for $R_f = 1$ (*dried sample*) ($R = 500$)

Table 5 Final hydrodynamic diameter of the magnetic particles obtained for various R_f ($R = 500$)

Exp.	D_h (nm)
$R_f = 0$	272
$R_f = 1/6$	300
$R_f = 1/3$	310
$R_f = 1$	322

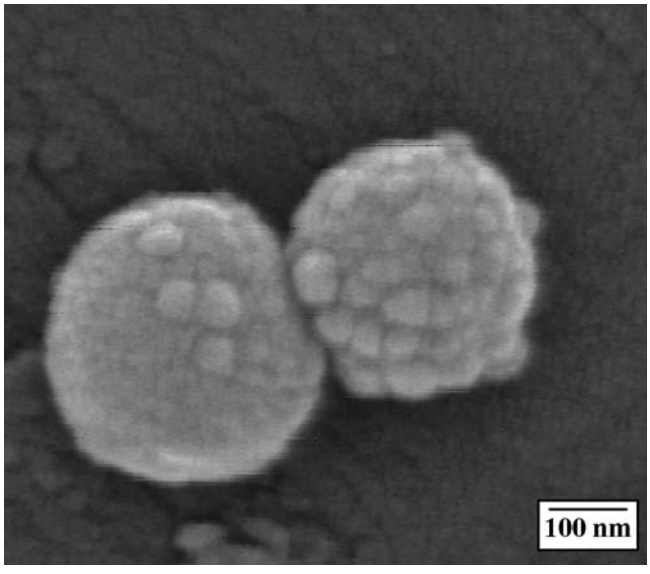

Fig. 8 Enlargement of SEM photo of magnetic particles obtained for $R_f = 1/6$ ($R = 500$)

spreading of the film-forming nanoparticles. Hence, these particles were likely to be embodied in the acrylic film, keeping their spherical shape as evidenced by the SEM photos displayed in Fig. 6. Moreover, higher the R_f, the better was the coverage of the magnetic droplets with the fluospheres.

As evidenced by Fig. 7 for $R_f = 1$, all the magnetic particles seemed to be fluorescent. However their intensity may not be constant from one particle to another, which may be related to the inhomogeneous distribution of the fluospheres among the particles, as shown by Fig. 8. Preliminary flow cytometry analyses were carried out in order to quantify the fluorescence of the final magnetic particles. For $R_f = 1$, four particles out of five were fluorescent. Also, the fluorescence distribution among the particles was reasonably good.

Complementary analyses were performed by TEM (Fig. 9). As already evidenced by the SEM photos, fluospheres were clearly distinguishable on the surface of the particles. This gave an uneven aspect to the surface in contrast to the particles formed in the absence of fluospheres. However, it was hard to see whether the encapsulating shell formed by the film-forming particles covered the entire surface comprising the magnetic droplets and the fluorescent nanoparticles. To increase the thickness of the encapsulating shell, an experiment was carried out with the same number of fluospheres as for the one where $R_f = 1$, but with twice film-forming particles, which implied $R_f = 0.5$ and $R = 765$. Unfortunately, even if the number of fluospheres was identical in the two experiments, the relative ratio of the introduced fluospheres was less compared to the whole of the nanoparticles. Their probability of adsorption was thus reduced as proven by the final particle size ($D_h = 296$ nm, against 322 nm) and the TEM photos (Fig. 10), which showed a lower coverage of the magnetic core with fluorescent nanoparticles. As demonstrated above (Table 5), the final particle size could be correlated with the initial amount of fluospheres and this behavior may be directly related to the nature of the fluospheres which did not spread during the film-formation step. The flow cytometry confirmed these observations: only 68% of the final particles were fluorescent (against 79% in the previous case), even if the fluorescence distribution was somewhat better.

Finally, preliminary thermogravimetric analyses were performed on the final composite particles in order to evaluate the magnetite content, which was found to be 76 wt% (data not shown).

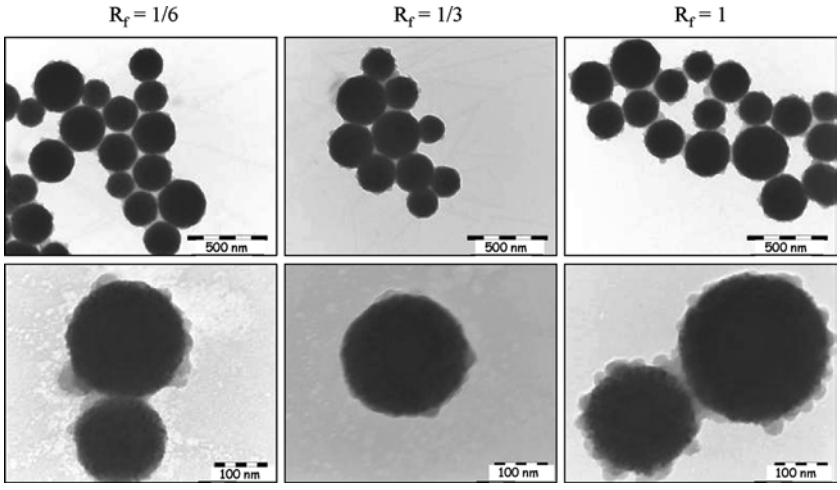

Fig. 9 TEM photos obtained for different ratios R_f ($R = 500$)

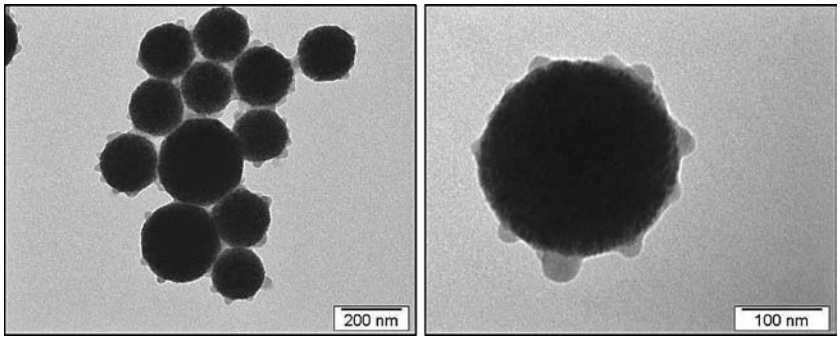

Fig. 10 TEM photos obtained for $R_f = 0.5$ and $R = 765$

Conclusions

This work aimed at elaborating fluorescent and magnetic submicronic particles displaying a large amount of magnetic material together with a fairly narrow particle size distribution. This was achieved by a stepwise heterocoagulation based strategy. The main results can be summarized as follows.

1. PEI adsorption was performed onto magnetic droplets so as to bring cationic surface charges. It was shown that conditions such as a PEI concentration of 50 mg mL^{-1} at alkaline pH led to the expected charge inversion while keeping efficient the colloidal stability of the magnetic emulsion. It was postulated that PEI adsorption resulted from a combination of both electrostatic interactions and hydrogen bonding. Each of this interaction may be predominant depending on pH and PEI concentration. Due to the complexity of the magnetic emulsion interface, more work is currently under progress in order to understand how PEI molecules interact with the magnetic droplets.
2. Anionic nanoparticles were then adsorbed onto the cationic magnetic droplets, followed by the encapsulation of the magnetic core by the spreading of the low T_g nanoparticles. The influence of the ratio of small to large particles, $R = N_S/N_L$, was investigated and stable systems were obtained for a value of 500 which turned out to be the best compromise between particle size, particle size distribution and the amount of film-forming nanoparticles. The efficient encapsulation of the particles was checked by electron microscopy.
3. Fluorescent polystyrene nanoparticles could be successfully incorporated together with the film-forming ones in order to elaborate core-shell like labeled magnetic particles. For this, R_f, the initial ratio of the fluorescent nanoparticles to the film-forming ones, was varied while keeping $R = 500$, showing that higher the R_f, the higher was the final particle size. The adsorption of fluospheres was also evidenced by electron microscopy and 80% of the final composite particles were found to be fluorescent.

In conclusion, the stepwise heterocoagulation process, which was found to be very easy to handle, efficient and reproducible, led to the formation of stable fluorescent and magnetic particles with high magnetite content, displaying a large specific surface area. Such particles should be good candidates as solid phase supports for biomolecules.

Acknowledgements The authors would like to thank Ademtech SA (Pessac, France) for providing magnetic emulsions, Rhodia (F. Leising) for the film-forming nanolatexes and Coatex (J.-M. Suau) for the amphiphilic copolymer. The financial support of the Agence Nationale de Valorisation de la Recherche is acknowledged. The authors are also grateful to S. Braconnot for his help in electron microscopy.

References

1. Halbreich A, Roger J, Pons JN, Da Silva MF, Bacri JC (2001) In: Arshady R (ed) Microspheres, microcapsules and liposomes, vol 3. Radiolabeled and magnetic particulates in medicine and biology. Citus Books, London, pp 459–493
2. Elaissari A, Sauzedde F, Montagne F, Pichot C (2003) In: Elaissari A (ed) Colloidal polymers: synthesis and characterization. Marcel Dekker, New York, pp 285–318
3. Gu S, Shiratori T, Konno M (2003) Colloid Polym Sci 281:1076
4. Liu ZL, Ding ZH, Yao KL, Tao J, Du GH, Lu QH, Wang X, Gong FL, Chen X (2003) J Magn Magn Mater 265:98
5. Ramirez LP, Landfester K (2003) Macrom Chem Phys 204:22
6. Montagne F, Braconnot S, Mondain-Monval O, Pichot C, Elaissari A (2003) J Disp Sci Tech 24:821
7. Caruso F, Spasova M, Susha A, Giersig M, Caruso RA (2001) Chem Mater 13:109
8. Voigt A, Buske N, Sukhorukov GB, Antipov AA, Leporatti S, Lichtenfeld H, Bäumler H, Donath E, Möhwald H (2001) J Magn Magn Mater 225:59
9. Furusawa K, Nagashima K, Anzai C (1994) Colloid Polym Sci 272:1104
10. Sauzedde F, Elaissari A, Pichot C (1999) Colloid Polym Sci 277:846 and Colloid Polym Sci 277:1041
11. Vincent B, Young CA, Tadros TF (1978) Faraday Discuss Chem Soc 65:296
12. Goodwin JW, Ottewill RH (1978) Faraday Discuss Chem Soc 65:338
13. Ottewill RH (1982) In: Piirma I (ed) Emulsion polymerization. Academic, New York, pp 36–38
14. Furusawa K, Anzai C (1987) Colloid Polym Sci 265:882
15. Okubo M, Ichikawa K, Tsujihiro M, He Y (1990) Colloid Polym Sci 268:791
16. Ottewill RH, Schofield AB, Waters JA (1996) Colloid Polym Sci 274:763
17. Ottewill RH, Schofield AB, Waters JA, Williams NStJ (1997) Colloid Polym Sci 275:274
18. Okubo M, Lu Y (1996) Colloids Surfaces A Physicochem Eng Aspects 109:49
19. Montagne F, Mondain-Monval O, Pichot C, Mozzanega H, Elaissari A (2002) J Magn Magn Mater 250:302
20. Ganachaud F, Mouterde G, Delair T, Elaissari A, Pichot C (1995) Polym Adv Tech 6:480
21. Hunter RJ (1981) In: Ottewill RH, Rowell RL (eds) Zeta potential in colloid science, principles and applications. Academic, London
22. Suh J, Paik HJ, Hwang BK (1994) Bioorg Chem 22:318
23. Koper GJM, van Duijvenbode RC, Stam DDP, Steuerle U, Borkovec M (2003) Macromolecules 36:2500
24. Hostetler RE, Swanson JW (1974) J Polym Sci Polym Chem Ed 12:29
25. Akari S, Schrepp W, Horn D (1996) Ber Bunsenges Phys Chem 100:1014
26. Li H, Han J, Panioukhine A, Kumacheva E (2002) J Colloid Interface Sci 255:119
27. Hansen FK, Matijevic E (1980) JSC Faraday I 76:1240
28. Vincent B, Young CA, Tadros TF (1980) JCS Faraday I 76:665
29. Li H, Kumacheva E (2003) Colloid Polym Sci 281:1
30. T_g (Polystyrene) = 100°C (1999) In: Brandrup J, Immergut EH, Grulke EA (ed) Polymer handbook, 4th edn. Wiley, Wiley Interscience, New York